Article | Received 22 June 2026; Revised 5 August 2026; Accepted 1 August 2026; Published X August 2026
https://doi.org/10.55092/mt20260005

A single-source domain generalization method based on frequency-domain statistical priors and class-conditional representation alignment for bearing fault diagnosis

Ning Jia[1,2], Changqing Shen[1,2], Zhongkui Zhu[1,2] and Weiguo Huang[1,2,*]

[1] School of Rail Transportation, Soochow University, Suzhou, China
[2] Intelligent Urban Rail Engineering Research Center of Jiangsu Province, Soochow University, Suzhou, China

* Correspondence author; E-mail: wghuang@suda.edu.cn.

Highlights:

- Interpretable frequency statistics become semantic anchors for deep features.
- Class-conditional alignment couples same-class priors and deep representations.
- Source-only training generalizes to unseen speeds without target-domain data.

Abstract: Rotating components in aviation equipment are subject to pronounced distribution shifts under different rotational speeds, loads, and installation conditions. As a result, conventional deep diagnostic models often suffer from performance degradation when deployed beyond the training operating condition. To address the practical constraint that target-domain samples are unavailable in advance and only one source operating condition can be used for training, this paper proposes a bearing fault diagnosis method that integrates frequency-domain statistical priors with class-conditional representation alignment. The one-dimensional vibration signal is transformed into both a frequency-domain amplitude spectrum and a two-dimensional time-frequency representation. The former is used to construct low-dimensional physical statistical descriptors, including center frequency, standard-deviation frequency, root-mean-square frequency, and kurtosis frequency, whereas the latter is fed into a convolutional network to extract deep discriminative representations. During training, a class-conditional prior-deep representation alignment constraint is introduced to pull the deep features of samples from the same class toward their corresponding frequency-domain prior representations while suppressing interference from priors of different classes. The two types of features are then concatenated and fed into a classifier for fault identification. Cross-condition experiments on a bearing dataset demonstrate that the proposed method improves diagnostic stability under unseen operating conditions without using target-domain training samples, thereby providing an interpretable modeling scheme for health monitoring of aviation equipment in high-cost and limited-source scenarios.

Keywords: aviation equipment; bearing fault diagnosis; single-source domain generalization; frequency-domain statistical prior; contrastive learning

1. Introduction

Aero-engines, transmission systems, and airborne auxiliary equipment contain a large number of high-speed rotating components. Their operating states are directly related to equipment safety, maintenance cost, and mission continuity [1,2]. As a typical load-bearing and transmission element, a bearing transmits fault-induced impacts through the structure once defects occur on the inner race, outer race, or rolling elements, and these impacts are further reflected in vibration signals. Therefore, condition monitoring and intelligent diagnosis of aviation bearings are of direct engineering significance for improving predictive maintenance of aviation equipment [3,4].

Deep learning has been widely applied to mechanical fault identification in recent years. Convolutional neural networks, attention-based models, and adversarial learning frameworks can automatically learn nonlinear features from vibration signals or time-frequency images, and they usually achieve high accuracy under independent and identically distributed testing conditions [5]. However, practical aviation equipment operates in complex environments. Rotational-speed combinations, load levels, sensor locations, and assembly states may all alter the signal distribution. When the training data cover only a limited number of operating conditions, the generalization capability of a diagnostic model under unseen conditions is often difficult to guarantee [6,7]. Domain generalization provides an important solution to this problem [8]. Multi-source domain generalization methods aim to learn condition-invariant representations from multiple source domains simultaneously so that stable performance can be maintained in unseen target domains. Wang *et al.* [9] designed a domain generalization network with multidomain-specific auxiliary classifiers, in which domain-specific information is first extracted from different source domains, domain-related features are then suppressed by a convolutional autoencoder, and generalizable diagnostic knowledge is finally learned through a domain-invariant classifier. Ma *et al.* [10] proposed a multi-source domain generalization method for fault diagnosis from the perspective of causal learning. Their method mines potential causal features through feature-diversity activation and uses a domain-discriminator-guided feature suppression mechanism to weaken non-causal interference, thereby improving robustness under unknown operating conditions. Gao *et al.* [11] further developed a deep adversarial domain generalization method based on multiple-classifier inconsistency, where Wasserstein distance is used to measure the output discrepancy among multi-source classifiers and adversarial training is employed to achieve fine-grained global feature alignment, enhancing cross-condition diagnosis of rotating systems. Nevertheless, in aviation-equipment experiments, the acquisition of multi-condition, multi-fault, and long-sequence data is costly, and some data may also be constrained by test conditions and engineering confidentiality. It is therefore difficult to construct a sufficiently rich multi-source training set. In contrast, single-source domain generalization (SDG) is more consistent with early-stage testing, few-sample deployment, and initial service of new equipment, but it is also more challenging: the model can observe only one source domain and lacks explicit cross-domain discrepancy samples to regularize feature learning [12]. Sun *et al.* [13] proposed a generic SDG framework based on wavelet packet augmentation and pseudo-domain generation. Their method augments samples through wavelet-packet decomposition and reconstruction and expands the source-domain distribution through pseudo-domain generation, thus improving robustness under unseen conditions. Huang *et al.* [14] designed an intra-domain self-generalization network (IDAN), which mines generalizable diagnostic information from multiscale features within a single source domain through a view-sharing strategy and optimizes the classification boundary using collaborative decision-making, thereby improving bearing diagnosis under unseen working conditions. Li *et al.* [15] proposed a dual adversarial and contrastive network (DACN), which simulates unknown-pattern features through adversarial pseudo-sample feature generation and extracts cross-pattern invariant representations by combining contrastive learning with adversarial training, enabling fault-diagnosis generalization from a single seen pattern to multiple unseen patterns. Existing studies usually improve the extrapolation capability of single-source models through pseudo-domain generation, data augmentation, or adversarial regularization. Although these strategies can increase training-sample diversity, they may also introduce distorted generated distributions, complex network structures, and increased computational costs. More importantly, purely data-driven models have limited ability to represent fault mechanisms, making it difficult to explain their decision basis to engineers. Aviation-equipment diagnosis therefore requires a closer integration of physical statistical knowledge from signal processing and adaptive representation learning from deep models.

Although frequency-prior learning, contrastive representation learning, and single-source domain generalization have been investigated separately, their roles differ from that of the proposed method. Existing frequency-prior methods generally introduce fault-frequency knowledge or spectral descriptors as additional inputs, attention guidance, or features directly supplied to a fusion classifier. In such methods, the prior mainly contributes to feature enhancement or final prediction. Conventional contrastive-learning methods typically construct positive pairs from augmented samples or different learned views of the same signal, without explicitly using an interpretable physical descriptor as the comparison target. In addition, existing single-source domain-generalization methods commonly enlarge the source distribution through data augmentation or pseudo-domain generation, or learn invariant features through adversarial regularization. In contrast, the proposed method treats four frequency-domain statistical descriptors as heterogeneous semantic anchors. These descriptors are projected into the deep-feature space and participate directly in a class-conditional cross-representation alignment loss, in which same-class deep-prior pairs are pulled together and different-class pairs are separated. Therefore, the contribution of this study lies in the source-only coupling and optimization mechanism between physical statistical priors and time-frequency deep representations, rather than in the individual use of frequency-domain features, feature fusion, or contrastive learning.

Based on the above considerations, this paper reorganizes the single-source bearing fault diagnosis problem and proposes a dual-channel representation learning framework constrained by frequency-domain statistical priors (FSP). The framework does not rely on target-domain data or require the construction of multiple additional source domains. Instead, it mines transferable information from within a single source domain. On the one hand, frequency-domain statistics are used to describe stable regularities associated with fault excitations. On the other hand, a time-frequency convolutional branch is used to learn complex local textures, and a class-conditional alignment loss is further introduced to establish the correspondence between these two types of representations. The main contributions of this paper are summarized as follows.

(1) A FSP branch is constructed for aviation-bearing signals. Physically meaningful spectral statistical indicators are converted into low-dimensional representations that can participate in network optimization, thereby improving model interpretability.

(2) A class-conditional prior-deep representation alignment constraint is designed to enhance the consistency between frequency-domain priors and deep features for samples from the same class

while maintaining sufficient margins between samples from different classes, thereby improving cross-condition discriminability.

(3) A dual-channel fusion classification procedure is established. Its effectiveness is validated on cross-speed tasks of an aero-engine bearing dataset, and its generalization advantages are analyzed in terms of accuracy, F1-score, and feature distribution.

2. Method

2.1. Problem formulation of single-source domain generalization diagnosis

Assume that only one source-domain dataset $D_s=\{(x_i,y_i)\}_{i=1}^{N_s}$ is available during training, where x_i denotes a vibration signal collected under a certain rotational-speed combination and y_i is the corresponding fault-class label. The target domain D_t encountered during testing shares the same label space as the source domain but follows a different operating-condition distribution, and samples from D_t are not involved in training. The objective of single-source domain generalization diagnosis is to learn a diagnostic function $F(\cdot)$ using only D_s so that high recognition accuracy can still be maintained in unseen target domains.

Unlike unsupervised transfer learning, this study does not assume that unlabeled target-domain data are observable. Unlike multi-source domain generalization, it also does not introduce multiple source operating conditions for joint training. Therefore, the model must extract more stable fault information from a single source domain and reduce its dependence on source-condition-specific patterns.

2.2. Overall framework

The proposed framework consists of a frequency-domain statistical prior branch, a time-frequency deep representation branch, a class-conditional representation alignment module, and a fusion classifier, as shown in Figure 1. For each one-dimensional vibration sample, the frequency-domain amplitude spectrum is first obtained by fast Fourier transform, and several spectral statistics are calculated as prior features. Meanwhile, the original signal is mapped into a two-dimensional time-frequency image using continuous wavelet transform, and deep features are extracted by a convolutional network. To enforce semantic consistency between the two representations, a prior-deep alignment loss is constructed during training and jointly optimized with the classification cross-entropy loss.

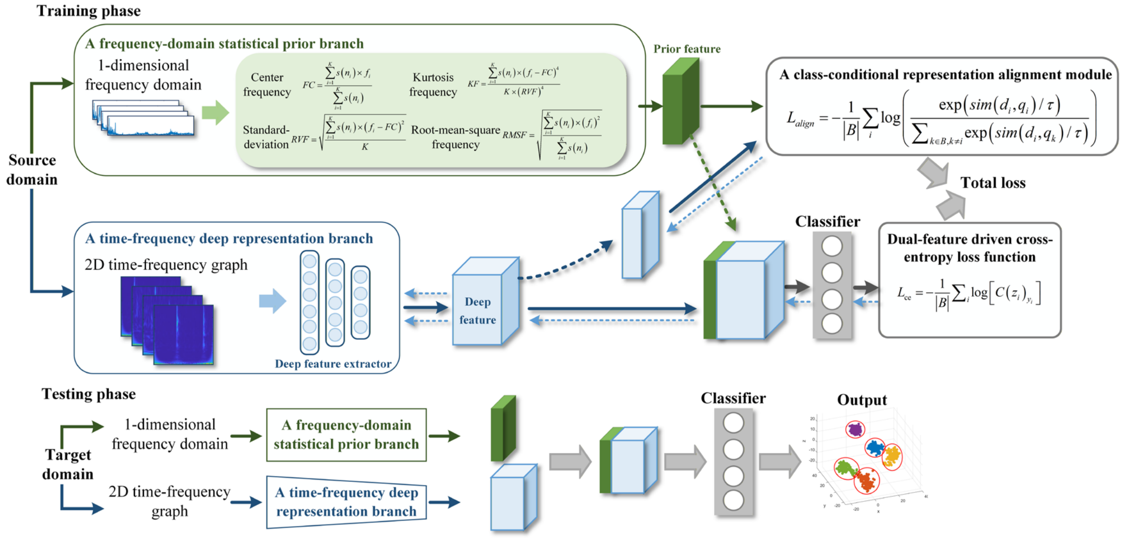

Figure 1. The proposed framework.

The key characteristic of this procedure is that the prior branch acts as a stable constraint rather than simply providing handcrafted features to the classifier. Frequency-domain statistics provide interpretable information related to fault excitation, whereas the deep branch characterizes local textures and high-order combinations in nonstationary signals. Through alignment learning, the two branches become complementary, enabling the model to better resist distribution shifts under unseen speed combinations.

2.3. Construction of frequency-domain statistical priors

Bearing faults introduce impact components and modulation phenomena into vibration signals, and these changes usually affect the spectral energy distribution. Compared with directly learning high-dimensional spectra, several statistical indicators can describe the spectral centroid, dispersion, and peak characteristics in a more compact manner. Given a time-domain signal $x(t)$, the amplitude spectrum $s(f_k)$ is obtained by *FFT*, where f_k denotes the *k*-th frequency point and *K* is the total number of frequency points. Four typical frequency-domain statistics are selected to form the prior vector p_i [16], as shown in Table 1.

To facilitate alignment with deep features, the prior vector is projected through a linear mapping:

$$q_i = W_p p_i + b_p \tag{1}$$

Where, $p_i \in \mathbb{R}^4$, $W_p \in \mathbb{R}^{d\times 4}$, $b_p \in \mathbb{R}^d$, and $q_i \in \mathbb{R}^d$. The output dimension d is set equal to the dimension of the deep representation, thereby enabling direct similarity calculation between the two representations. This mapping does not change the physical definition of the priors; it only transforms the low-dimensional statistical vector into a feature space compatible with the deep representation.

Table 1. Frequency-domain statistical prior features.

Feature	Expression	Description
Center frequency (FC)	$FC = \dfrac{\sum_{i=1}^{K} s(n_i)\times f_i}{\sum_{i=1}^{K} s(n_i)}$	Centroid position of the spectral energy distribution
Standard-deviation frequency (RVF)	$RVF = \sqrt{\dfrac{\sum_{i=1}^{K} s(n_i)\times (f_i - FC)^2}{K}}$	Dispersion of frequency components around the center frequency
Root-mean-square frequency (RMSF)	$RMSF = \sqrt{\dfrac{\sum_{i=1}^{K} s(n_i)\times (f_i)^2}{\sum_{i=1}^{K} s(n_i)}}$	Overall level of spectral energy along the frequency axis
Kurtosis frequency (KF)	$KF = \dfrac{\sum_{i=1}^{K} s(n_i)\times (f_i - FC)^4}{K\times (RVF)^4}$	Sensitivity to spectral peaks and impulsive components

2.4. Time-frequency deep representation branch

To capture the time-varying frequency structure of nonstationary fault signals, this paper converts the one-dimensional vibration signal into a two-dimensional time-frequency image. The time-frequency image preserves both the temporal location of impacts and the corresponding frequency-response characteristics, making it suitable for local pattern extraction by convolutional networks. The deep representation branch adopts convolution, normalization, pooling, and nonlinear activation as its basic units, and its output is denoted as $d_i = G_d\left(T\left(x_i\right)\right)$, where $T(\cdot)$ represents the time-frequency transform.

The network follows a lightweight convolutional feature-extraction design. Larger kernels in the shallow layers are used to capture broadband local responses, whereas smaller kernels in subsequent layers progressively abstract high-level fault textures. To remain consistent with the original experimental setting, the input time-frequency image is resized to 227 × 227 × 3. The detailed configuration is shown in Table 2.

Table 2. Architecture of the time-frequency deep feature extractor.

Layer	Type	Parameters and operations
data	Image input layer	Input size: 227 × 227 × 3
conv1	2D convolution + ReLU	11 × 11 kernel, 96 filters, stride 4
norm1	Cross-channel normalization	Channel window size: 5
pool1	Max pooling	3 × 3 pooling kernel, stride 2
conv2	Grouped convolution + ReLU	5 × 5 kernel, 2 groups, 128 filters per group
norm2	Cross-channel normalization	Channel window size: 5
pool2	Max pooling	3 × 3 pooling kernel, stride 2
conv3	2D convolution + ReLU	3 × 3 kernel, 384 filters
conv4	Grouped convolution + ReLU	3 × 3 kernel, 2 groups, 192 filters per group
conv5	Grouped convolution	3 × 3 kernel, 2 groups, 128 filters per group

2.5. Class-conditional prior-deep representation alignment

Simply concatenating prior features with deep features cannot ensure that the two representations form a consistent class structure in the semantic space. Therefore, this paper constructs a class-conditional representation alignment constraint within each mini-batch. For the deep representation d_i of sample *i*, the prior projections q_j of samples with the same label are treated as positives, whereas the prior projections q_k of samples from other classes are treated as negatives. Cross-representation distance is calculated using cosine similarity $sim(\cdot)$, so that the deep branch is encouraged during optimization to focus on frequency-domain priors that are stably related to fault classes.

$$L_{align} = -\frac{1}{|B|}\sum_{i}\log\left(\frac{\exp\left(sim\left(d_i, q_i\right)/\tau\right)}{\sum_{k\in B, k\neq i}\exp\left(sim\left(d_i, q_k\right)/\tau\right)}\right) \tag{2}$$

Where, B denotes the current mini-batch, q_i is the set of samples that have the same label as sample *i*, and τ is the temperature coefficient. A smaller τ makes the model more sensitive to similarity differences. This paper adopts the commonly used setting τ = 0.07. This constraint essentially transforms interpretable handcrafted statistics into class-structure supervision, enabling the deep network to learn representations that are less dependent on a single operating condition.

2.6. Fusion classification and joint optimization

After prior projection and deep feature extraction, the two representations are concatenated to obtain the fused feature $z_i = Concat(d_i, q_i)$, which is then fed into the classifier $C(\cdot)$ to output fault-class probabilities. The classification loss is defined as the cross-entropy loss:

$$L_{ce} = -\frac{1}{|B|}\sum_i \log\left[C(z_i)_{y_i}\right] \tag{3}$$

The final objective function consists of the classification loss and the representation alignment loss:

$$\begin{aligned} L &= L_{ce} + \lambda L_{align} \\ &= -\frac{1}{|B|}\sum_i \log\left[C(z_i)_{y_i}\right] + \lambda\left\{-\frac{1}{|B|}\sum_i \log\left(\frac{\exp(sim(d_i, q_i)/\tau)}{\sum_{k\in B, k\neq i}\exp(sim(d_i, q_k)/\tau)}\right)\right\} \end{aligned} \tag{4}$$

During training, the time-frequency deep branch, the prior projection layer, and the classifier are updated simultaneously. During testing, only the target-domain signal is required; the same frequency-domain statistical calculation and time-frequency convolutional extraction procedure is applied to obtain the diagnostic result, without any target-domain sample participating in parameter updating. The value of λ determined based solely on the source-domain validation results, without using any target-domain samples for hyperparameter selection.

3. Experimental design

3.1. Dataset and preprocessing

3.3.1. Harbin institute of technology aero-engine bearing dataset

The experiments are conducted on the Harbin Institute of Technology aero-engine bearing dataset [17]. The test rig uses a dual-motor drive to simulate the dual-rotor structure of an aero-engine, and vibration signals can be collected under different combinations of low-pressure and high-pressure rotor speeds. The dataset contains four health states: healthy, outer-race fault, slight inner-race fault, and severe inner-race fault. These states reflect typical degradation modes of aviation intermediate bearings under varying operating conditions. Three speed combinations are selected to construct cross-condition tasks: LP1000 r/min-HP1200 r/min, LP3000 r/min-HP3600 r/min, and LP4000 r/min-HP4800 r/min. The sampling frequency is 25,000 Hz.

3.3.2. Jiangnan university bearing dataset

The experiments are also conducted on the open Jiangnan University (JNU) bearing dataset [18]. The dataset contains four health states: healthy, inner-race fault, outer-race fault, and rolling-element fault. Vibration acceleration signals were collected under three rotational speeds: 600 r/min, 800 r/min, and 1000 r/min. These speed conditions are used to construct single-source cross-condition tasks, in which one speed condition serves as the source domain and another unseen speed condition serves as the target domain. The sampling frequency is 50 kHz. Owing to the distribution differences caused by rotational-speed variations, the JNU dataset provides an additional benchmark for evaluating the cross-speed generalization capability of the proposed method.

3.3.3. Data preprocessing

The samples are segmented using a sliding window with a length of 2048. For each operating condition, 200 samples are selected for each class, resulting in 800 samples in total. The frequency-domain branch calculates prior statistics from the FFT amplitude spectrum, while the deep branch generates two-dimensional time-frequency images using the mor3-3 wavelet function.

3.2. Single-source domain generalization task settings

To evaluate generalization under unseen operating conditions, only one speed combination is used to train the model each time, and another speed combination is used entirely as the target-domain test set. The twelve single-source cross-domain tasks are listed in Table 3. All compared methods are repeated ten times under the same data partition, and the average results are reported to reduce the influence of random initialization and batch sampling.

Table 3. Single-source domain generalization tasks.

	HIT dataset	
Task	**Source domain/training samples**	**Target domain/testing samples**
H1	LP1000-HP1200 [200 × 4 = 800]	LP3000-HP3600 [200 × 4 = 800]
H2	LP1000-HP1200 [200 × 4 = 800]	LP4000-HP4800 [200 × 4 = 800]
H3	LP3000-HP3600 [200 × 4 = 800]	LP1000-HP1200 [200 × 4 = 800]
H4	LP3000-HP3600 [200 × 4 = 800]	LP4000-HP4800 [200 × 4 = 800]
H5	LP4000-HP4800 [200 × 4 = 800]	LP1000-HP1200 [200 × 4 = 800]
H6	LP4000-HP4800 [200 × 4 = 800]	LP3000-HP3600 [200 × 4 = 800]
	JNU dataset	
Task	**Source domain/training samples**	**Target domain/testing samples**
J1	600rpm [200 × 4 = 800]	800 rpm [200 × 4 = 800]
J2	600 rpm [200 × 4 = 800]	1000 rpm [200 × 4 = 800]
J3	800 rpm [200 × 4 = 800]	600 rpm [200 × 4 = 800]
J4	800 rpm [200 × 4 = 800]	1000 rpm [200 × 4 = 800]
J5	1000 rpm [200 × 4 = 800]	600 rpm [200 × 4 = 800]
J6	1000 rpm [200 × 4 = 800]	800 rpm [200 × 4 = 800]

3.3. Implementation details

The model is trained with a learning rate of 0.0001, a batch size of 32, training epochs of 15, a momentum of 0.9, and a weight decay of 0.01. The experiments are implemented on a workstation equipped with an Intel® Core™ i5-13400F CPU and a GeForce RTX™ 4090 GPU. The data acquisition software was developed based on LabVIEW®. Signal processing and data mining were carried out using MATLAB®. To ensure a fair comparison, all methods use the same sample partition, input length, and evaluation metrics.

3.4. Compared methods and comparative experimental analysis

The compared methods include: (1) WDCNN, which enhances raw-signal feature extraction through a wide convolutional kernel [19]; (2) DATN, which reduces domain discrepancy through an adversarial mechanism [20]; (3) Mixup, which expands the training distribution by interpolating samples and labels [21]; (4) AMINet, which introduces mutual-information adversarial constraints for single-source domain generalization [22]; and (5) SDIGN, which expands single-source training information through incremental pseudo-domain generation [23]. These methods cover deep baselines, transfer/adversarial learning, data augmentation, and single-source generalization generation strategies, and thus provide a comprehensive evaluation of the proposed method.

Table 4 summarizes the average diagnostic accuracy of different methods on the cross-condition tasks of the HIT (H1–H6) and JNU (J1–J6) datasets. Table 5 shows the F1 scores of different methods on the single-source domain generalization task. On the HIT dataset, the proposed method improves the average accuracy by 2.17–22.31 percentage points compared with the other methods, indicating that frequency-domain statistical priors and deep representation alignment can effectively alleviate operating-condition shifts under single-source training. On the independent JNU dataset, the proposed method achieves an average accuracy of 92.17%, outperforming the strongest baseline, SDIGN, by 4.82 percentage points and obtaining the highest accuracy in all six tasks**.** Particularly in tasks involving relatively large speed differences, methods that rely solely on deep convolutional features are more likely to capture source-condition-specific texture patterns, whereas the proposed method retains stable information related to fault mechanisms through the prior constraint. The consistent results on two bearing test platforms further indicate that the effectiveness of the proposed method is not restricted to the original aero-engine bearing dataset.

Table 4. Diagnostic accuracy of different methods on single-source domain generalization tasks/%. Bold indicates the optimal result.

Method	**H1**	**H2**	**H3**	**H4**	**H5**	**H6**	**Average**
WDCNN	74.31	78.18	62.51	65.72	70.84	78.09	71.61
DATN	83.79	85.55	65.62	81.36	81.07	86.87	80.71
Mixup	86.46	88.97	69.48	84.29	84.63	88.03	83.64
AMINet	89.61	93.22	74.57	86.41	87.44	88.36	86.60
SDIGN	90.39	94.05	90.22	89.37	92.14	94.31	91.75
Proposed	**93.37**	**96.16**	**92.35**	**92.18**	**93.52**	**95.96**	**93.92**
Method	**J1**	**J2**	**J3**	**J4**	**J5**	**J6**	**Average**
WDCNN	73.78	61.49	64.60	77.93	62.40	74.60	69.13
DATN	82.45	80.48	66.91	89.14	76.66	87.34	80.50
Mixup	84.91	81.84	65.35	89.86	74.27	84.53	80.13
AMINet	88.15	83.02	74.19	92.65	77.15	90.48	84.27
SDIGN	90.48	87.17	87.28	91.98	78.02	89.15	87.35
Proposed	**96.18**	**92.98**	**92.98**	**94.62**	**82.27**	**93.98**	**92.17**

Table 5. F1-scores of different methods on single-source domain generalization tasks. Bold indicates the optimal result.

Method	**H1**	**H2**	**H3**	**H4**	**H5**	**H6**	**Average**
WDCNN	73.62	77.54	61.83	65.08	70.21	77.42	70.95
DATN	83.06	84.91	64.87	80.68	80.35	86.19	80.01
Mixup	85.78	88.31	68.74	83.62	83.91	87.36	82.95
AMINet	88.94	92.57	73.89	85.76	86.71	87.68	85.93
SDIGN	89.72	93.38	89.54	88.69	91.46	93.63	91.07
Proposed	92.71	95.49	91.66	91.54	92.84	95.31	93.26
Method	**J1**	**J2**	**J3**	**J4**	**J5**	**J6**	**Average**
WDCNN	73.02	61.50	64.62	78.65	61.61	74.05	68.91
DATN	82.56	81.05	67.01	89.60	77.20	87.84	80.88
Mixup	84.39	82.07	64.57	90.49	74.17	85.16	80.14
AMINet	88.51	82.44	73.69	93.61	78.01	91.09	84.56
SDIGN	90.51	86.32	86.96	92.09	77.60	89.06	87.09
Proposed	**96.59**	**93.13**	**92.03**	**95.04**	**82.00**	**93.82**	**92.10**

3.5. Ablation experiments and discussion

To clarify the roles of the proposed components, the ablation experiments are organized according to the two mechanisms through which the frequency-domain statistical prior participates in the model: feature fusion for classification and prior-deep alignment for representation regularization. All variants use the same time-frequency deep-feature extractor. Whenever the frequency-domain prior is introduced, the same linear projection layer is used to map the four-dimensional prior vector p_i to the d-dimensional representation q_i. Therefore, the projection layer serves only as a shared dimensional adapter and is not treated as an independent diagnostic component. The four ablation settings constitute a two-factor design that separately evaluates prior-based feature fusion and class-conditional representation alignment.

A1 (Deep features only): Only the time-frequency deep-feature extraction branch is retained. The classifier receives the deep representation h_i, and the model is optimized using only the cross-entropy loss. Neither frequency-domain priors nor the prior-deep alignment loss is introduced.

A2 (Prior fusion without alignment): The frequency-domain statistical prior is mapped to q_i using the same projection layer as that employed in the complete model. The projected prior representation q_i is concatenated with the deep representation h_i and fed into the classifier. The model is optimized using only the cross-entropy loss, with the alignment-loss weight set to zero. Therefore, A2 evaluates the contribution of prior-based feature fusion without class-conditional alignment.

A3 (Alignment without fusion): The projected prior representation q_i is used only to calculate the class-conditional prior-deep alignment loss during training. The classifier receives only the deep representation h_i, and q_i is not concatenated with h_i for classification. Therefore, A3 evaluates whether the prior-based alignment constraint improves the quality and generalization capability of the learned deep representation independently of feature fusion.

Taking the aero-engine bearing dataset as an example, the diagnostic results of the different ablation models are presented in Table 6. A1, which uses only the time-frequency deep representation for classification, achieves an average accuracy of 67.48% and serves as the baseline. Compared with A1, A2 improves the average accuracy to 81.60%, demonstrating that the projected frequency-domain statistical priors provide complementary fault information when fused with the time-frequency deep features. A3 achieves an average accuracy of 90.54%, which is 23.06 percentage points higher than A1, although its classifier still receives only the deep representation. This result indicates that the class-conditional prior-deep alignment constraint improves the generalization quality of the learned deep features rather than merely supplying additional prior features to the classifier. When the feature-fusion mechanism is retained, introducing the alignment constraint increases the average accuracy from 81.60% in A2 to 93.92% in the complete model. Conversely, under the same alignment constraint, incorporating the projected prior representation into the classifier improves the average accuracy from 90.54% in A3 to 93.92%. These controlled comparisons demonstrate that prior-based feature fusion and class-conditional representation alignment make distinct and complementary contributions to cross-condition fault diagnosis. The prior projection layer is consistently used as a dimensional-matching operation whenever the prior branch is activated and is therefore not regarded as an independent diagnostic module.

Table 6. Results of the ablation experiments.

Method	H1	H2	H3	H4	H5	H6	Average
A1	70.95	68.14	67.18	70.19	60.48	67.94	67.48
A2	81.18	83.95	81.49	76.48	80.87	85.60	81.60
A3	91.98	90.16	90.76	88.97	90.94	90.40	90.54
Proposed	93.37	96.16	92.35	92.18	93.52	95.96	93.92

4. Conclusions

To address the problems that target-domain data are unavailable and multi-source operating-condition samples are difficult to obtain in aviation bearing fault diagnosis, this paper proposes a single-source domain generalization diagnostic method that integrates frequency-domain statistical priors with class-conditional representation alignment. The method incorporates spectral statistical indicators and time-frequency deep features into a unified optimization framework. Through cross-representation alignment loss, it enhances intra-class consistency and inter-class separability without using target-domain training data, thereby improving diagnostic stability under unseen operating conditions. Experiments on the aero-engine bearing dataset show that the proposed method achieves better average diagnostic performance than typical deep learning, data augmentation, transfer learning, and single-source generalization methods.

This method can be applied to offline health assessment and early fault warning for key rotating components such as aero-engine bearings and airborne transmission systems, and shows good application prospects in aviation equipment maintenance scenarios with scarce fault samples and variable operating conditions. Future work may further investigate multi-type prior fusion, lightweight model deployment, and online diagnostic validation under real flight loads to promote the engineering application of the proposed method.

Data availability statement

No supplementary or additional data were generated in this study.

Declaration of generative AI and AI-assisted technologies

During the preparation of this manuscript, the authors used generative AI tools only to improve language and readability. Specifically, the authors used ChatGPT and Grammarly for language polishing only. The authors take full responsibility for the content of the manuscript. The authors take full responsibility for the content of the manuscript.

Acknowledgments

This work was supported in part by the National Natural Science Foundation of China under Grant 52475116, Grant 52272440, and Grant 52275121, and in part by the Jiangsu Qinglan Project.

Authors' contribution

Conceptualization: N.J. and W.H.; methodology: N.J.; software: N.J.; validation: N.J., W.H. and C.S.; formal analysis: N.J.; investigation: N.J.; resources: W.H. and Z.Z.; data curation: N.J.; writing—original

draft preparation: N.J.; writing—review and editing: N.J.; visualization: N.J.; supervision: W.H., C.S. and Z.Z.; project administration: W.H.; funding acquisition: W.H., C.S. and Z.Z. All authors have read and agreed to the published version of the manuscript.

Conflicts of interest

The authors declare that they have no known competing financial.

References

[1] Li T, Chen J, Liu T, Sun C, Zhao Z, *et al.* Explainable artificial intelligence based intelligent fault diagnosis: a systematic review from applications to insights. *Reliab. Eng. Syst. Saf.* 2026, 267:111935.

[2] Jia N, Huang W, Ding C, Wang J, Zhu Z. PC3Net: a prior-causal contrast-collaboration network for single domain generalization fault diagnosis. *Reliab. Eng. Syst. Saf.* 2025, 264:111411.

[3] Xu H, Hu C, Li Y, Zhou Z, Zhu Q, *et al.* A condition-supervised contrastive autoencoder with dynamic temperature scaling for anomaly detection under multi-condition imbalanced data. *Expert Syst. Appl.* 2026, 317:131990.

[4] Wang Z, Han G, Liu L, Wang F, Zhu Y. A globally interpretable convolutional neural network combining bearing semantics for bearing fault diagnosis. *IEEE Trans. Instrum. Meas.* 2025, 74:1–13.

[5] Liu X, Guo X, Yang H. A novel analogue circuit incipient soft fault diagnosis method based on a multiscale fault diagnosis network. *Circuits Syst. Signal Process.* 2025, 45(4):2475–2494.

[6] Zheng H, Yang Y, Yin J, Li Y, Wang R, *et al.* Deep domain generalization combining a priori diagnosis knowledge toward cross-domain fault diagnosis of rolling bearing. *IEEE Trans. Instrum. Meas.* 2020, 70:1–11.

[7] Li G, Wei M, Wu D, Cheng Y, Wu J, *et al.* Zero-sample fault diagnosis of rolling bearings via fault spectrum knowledge and autonomous contrastive learning. *Expert Syst. Appl.* 2025, 275:127080.

[8] Wen C, Zhang J, Wang Z, Liu W, Yang J. A novel multi-scale quadratic convolutional network for bearing fault diagnosis: Handling noisy conditions. *Knowl.-Based Syst.* 2025, 300:114614.

[9] Wang R, Huang W, Lu Y, Zhang X, Wang J, *et al.* A novel domain generalization network with multidomain specific auxiliary classifiers for machinery fault diagnosis under unseen working conditions. *Reliab. Eng. Syst. Saf.* 2023, 238:109463.

[10] Ma H, Wei J, Zhang G, Kong X, Du J. Causality-inspired multi-source domain generalization method for intelligent fault diagnosis under unknown operating conditions. *Reliab. Eng. Syst. Saf.* 2024, 252:110439.

[11] Gao L, Gao Q, Liu Z, Cheng H, Yao J, *et al.* Multiple classifiers inconsistency-based deep adversarial domain generalization method for cross-condition fault diagnosis in rotating systems. *Reliab. Eng. Syst. Saf.* 2025, 260:111017.

[12] Pan H, Chen C, Chen T, Cheng J, Zhang J, *et al.* A fuzzy cross domain matrix machine for fault diagnosis under multi-objective domain. *Eng. Appl. Artif. Intell.* 2026, 164:113368.

[13] Sun Y, Tao H, Ni Y, Stojanović V. A generic single-source domain generalization framework for fault diagnosis via wavelet packet augmentation and pseudo-domain generation. *IEEE Internet Things J.* 2025, 12(15):31629–31642.

[14] Huang K, Ren Z, Zhu L, Lin T, Zhu Y, *et al.* Intra-domain self generalization network for intelligent fault diagnosis of bearings under unseen working conditions. *Adv. Eng. Inf.* 2025, 64: 102997.

[15] Li G, Atoui MA, Li X. Dual adversarial and contrastive network for single-source domain generalization in fault diagnosis. *Adv. Eng. Inf.* 2025, 65:103140.

[16] Cui Y, Qin Y, Liu C, Wang P, Gao Y. A frequency-prior guided dual-attention and gated fusion network for intelligent bearing fault diagnosis. *Struct. Health Monit.* 2026.

[17] Hou L, Yi H, Jin Y, Gui M, Sui L, *et al*. Inter-shaft bearing fault diagnosis based on aero-engine system: a benchmarking dataset study. *J. Dyn. Monit. Diagn.* 2023, 2(4):228–242.

[18] Li K, Ping X, Wang H, Chen P, Cao Y. Sequential fuzzy diagnosis method for motor roller bearing in variable operating conditions based on vibration analysis. *Sensors* 2013, 13(6):8013–8041.

[19] Zhang W, Peng G, Li C, Chen Y, Zhang Z. A new deep learning model for fault diagnosis with good anti-noise and domain adaptation ability on raw vibration signals. *Sensors* 2017, 17(2):425.

[20] Chen Z, He G, Li J, Liao Y, Gryllias KC, *et al.* Domain adversarial transfer network for cross-domain fault diagnosis of rotary machinery. *IEEE Trans. Instrum. Meas.* 2020, 69(11):8702–8712.

[21] Wang Y, Li Z, Yu H, Li J. Mixup-based maximum distribution difference selection strategy for domain generalization. *Expert Syst. Appl.* 2025, 281:127521.

[22] Zhao C, Shen W. Adversarial mutual information-guided single domain generalization network for intelligent fault diagnosis. *IEEE Trans. Ind. Inf.* 2022, 19(3):2909–2918.

[23] Pu Y, Tang J, Li X, Wei C, Huang W, *et al.* Single-domain incremental generation network for machinery intelligent fault diagnosis under unknown working speeds. *Adv. Eng. Inf.* 2024, 60:102400.